THE JOURNAL OF BIOLOGICAL CHEMISTRY VOL. 281, NO. 12, pp. 7946–7951, March 24, 2006

The Molecular Circuitry Regulating the Switch between Iron Deficiency and Overload in Mice*[S]

Received for publication, September 7, 2005, and in revised form, December 26, 2005 Published, JBC Papers in Press, January 17, 2006, DOI 10.1074/jbc.M509857200

Henry Mok[‡§1], **Agnieszka E. Mlodnicka**[‡], **Matthias W. Hentze**[¶], **Martina Muckenthaler**[‖], **and Armin Schumacher**[‡2]

From the [‡]*Department of Molecular and Human Genetics and* [§]*Medical Scientist Training Program, Baylor College of Medicine, Houston, Texas 77030,* [¶]*European Molecular Biology Laboratory, 69117 Heidelberg, Germany, and the* [‖]*Department of Pediatric Oncology, Hematology, and Immunology, University of Heidelberg, 69120 Heidelberg, Germany*

Recent positional cloning of the radiation-induced polycythaemia (*Pcm*) mutation revealed a 58-bp microdeletion in the promoter region of ferroportin 1 (Fpn1), the sole cellular iron exporter identified to date. Here we report a molecular definition of the regulatory mechanisms governing the dynamic changes in iron balance in *Pcm* heterozygous mice between 3 and 12 weeks of age. Hepatic and/or duodenal response patterns of iron metabolism genes, such as *Trfr*, *cybrd1*, and *Slc11a2*, explained the transition from early postnatal iron deficiency to iron overload by 12 weeks of age. A significant delay in developmental up-regulation of *hepcidin* (*Hamp*), the pivotal hormonal regulator of iron homeostasis, correlated with high levels of Fpn1 expression in hepatic Kupffer cells and duodenal epithelial cells at 7 weeks of age. Conversely, upon up-regulation of *Hamp* expression at 12 weeks of age, Fpn1 expression decreased, indicative of a Hamp-mediated homeostatic loop. *Hamp* regulation due to iron did not appear dependent on transcription-level changes of the murine homolog of Hemojuvelin (*Rgmc*). Aged cohorts of *Pcm* mice exhibited low levels of Fpn1 expression in the context of an iron-deficient erythropoiesis and profound iron sequestration in reticuloendothelial macrophages, duodenum, and other tissues. Thus, similar to the anemia of chronic disease, these findings demonstrate decreased iron bioavailability due to sustained down-regulation of Fpn1 levels by Hamp. We conclude that regulatory alleles, such as *Pcm*, with highly dynamic changes in iron balance are ideally suited to interrogate the genetic circuitry regulating iron metabolism.

In mammals, iron bioavailability for erythropoiesis and other vital organismal functions is regulated at three principal sites: placental or duodenal uptake, release from hepatic stores, and recycling of scavenged iron from senescent red blood cells via reticuloendothelial (RES)[3] macrophages (1). Iron recycling from macrophages generates the vast majority of iron for daily consumption, amounting to ~22 mg of iron per day under steady state conditions in humans (2). Ferroportin 1 (Fpn1; also known as MTP1, IREG1, SLC11A3, SLC39A1) plays a pivotal role at all three sites and functions as the sole cellular iron exporter identified to date (3–5).

Both cellular and systemic hormonal mechanisms impinge upon Fpn1 regulation. Predominant modes of cellular regulation include transcriptional as well as translational control. Several studies document changes in Fpn1 mRNA levels and transcription rates in mice and cultured cells under conditions of iron overload or deficiency (6–14). Translational regulation involves a highly conserved sequence in the 5′-untranslated region of Fpn1 mRNA known as the iron-responsive element (1). *Trans*-acting iron regulatory proteins bind to the iron-responsive element stem-loop structure, inhibiting Fpn1 mRNA translation under low intracellular iron conditions in tissue culture cells (6, 7, 15). Hepcidin (Hamp), the principal hormonal regulator of iron homeostasis (1), controls Fpn1 expression levels at the cell surface by a post-translational mechanism. Upon Hamp binding to cell surface-bound Fpn1, the iron exporter becomes internalized and degraded in lysosomes (16). Importantly, this implicates the Hamp-Fpn1 axis in a homeostatic loop wherein, under conditions of high intracellular iron in hepatic stores, Hamp-mediated degradation of Fpn1 decreases duodenal iron uptake and macrophage iron release, preventing organismal iron overload.

Coding region mutations in human FPN1 cause the autosomal dominant ferroportin disease (also referred to as hemochromatosis, type IV) (17). Furthermore, two mutant mouse models for Fpn1 function were recently described (3, 5). Constitutive or conditional deletion of several transmembrane domains confirmed Fpn1 function in maternal-to-fetal iron transport, export from duodenal enterocytes, and iron release from RES macrophages (5). The other mouse model involves a regulatory allele of Fpn1 generated by radiation mutagenesis. Positional cloning identified a 58-bp microdeletion in the Fpn1 promoter in polycythaemia (*Pcm*) mutant mice (3). Depending on the developmental stage, tissue, and genotype, the microdeletion caused dynamic dysregulation of Fpn1 expression, resulting in both hypo- and hypermorphic phenotypes (3, 4). During late gestation, decreased Fpn1 protein expression in placental syncytiotrophoblast cells resulted in a severe neonatal iron deficiency and a hypochromic, microcytic anemia in *Pcm* homozygotes, providing the first definitive evidence for Fpn1 function in maternal-to-fetal iron transport in mammals (4). Postnatally, aberrant transcription initiation eliminated the iron-responsive element in the 5′-untranslated region of Fpn1 mRNA, increasing hepatic and duodenal Fpn1 protein levels (3). The latter governed augmentation of intestinal iron uptake, reversing the perinatal iron deficiency to a tissue iron overload by 12 weeks of age. Strikingly, the majority of *Pcm* heterozygous animals displayed a transient erythropoietin-dependent polycythaemia with peak hematocrits of up to 80% during young adulthood, eponymous of the mutant strain (3).

Here we report the molecular mechanisms underlying the iron homeostasis defects in *Pcm* mice. The "IronChip" microarray platform

* This work was supported in part by a National Institutes of Health research grant (to A. S.). The costs of publication of this article were defrayed in part by the payment of page charges. This article must therefore be hereby marked "*advertisement*" in accordance with 18 U.S.C. Section 1734 solely to indicate this fact.

[S] The on-line version of this article (available at http://www.jbc.org) contains supplemental Tables S1 and S2.

[1] Supported by an individual National Research Service Award from the NIEHS, National Institutes of Health and recipient of a National Institutes of Health training grant through the Dept. of Molecular and Human Genetics.

[2] To whom correspondence should be addressed: Dept. of Molecular and Human Genetics, Baylor College of Medicine, One Baylor Plaza, S-803, Houston, TX 77030. Tel.: 713-798-6865; Fax: 713-798-8985; E-mail: armins@bcm.tmc.edu.

[3] The abbreviations used are: RES, reticuloendothelial; HAMP, hepcidin; Pcm, polycythaemia; ΔCT, difference of cycles to threshold; Hct, hematocrit; WBC, white blood count; Trfr, transferrin receptor.

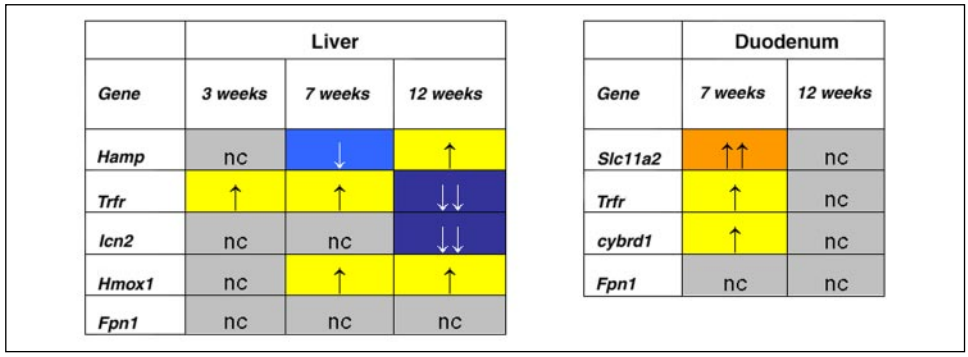

Liver			
Gene	3 weeks	7 weeks	12 weeks
Hamp	nc	↓	↑
Trfr	↑	↑	↓↓
Icn2	nc	nc	↓↓
Hmox1	nc	↑	↑
Fpn1	nc	nc	nc

Duodenum		
Gene	7 weeks	12 weeks
Slc11a2	↑↑	nc
Trfr	↑	nc
cybrd1	↑	nc
Fpn1	nc	nc

FIGURE 1. **Summary of the regulatory responses in liver and duodenum in *Pcm* heterozygous mice during postnatal development.** *Left* and *right panels* shows hepatic and duodenal gene expression, respectively. A subset of differentially expressed genes is listed. ↓ ↓ (*dark blue*) indicates a 2–5-fold decrease in mRNA levels. ↓ (*light blue*) indicates a decrease in mRNA levels between at least 1.3- and 1.9-fold. ↑ ↑ (*orange*) depicts a 2.5-fold increase in mRNA levels. ↑ (*yellow*) represents an increase in mRNA levels between at least 1.3- and 1.9-fold. *nc* (no change), no significant change in mRNA levels (<1.3-fold in either direction). *Icn2*, Lipocalin 2.

and real-time quantitative RT-PCR accurately defined the hepatic and duodenal gene response patterns that governed the transition from early postnatal iron deficiency to tissue iron overload in young adult *Pcm* mice. In support of a Hamp-Fpn1 homeostatic loop *in vivo*, *Pcm* mice manifested an inverse correlation between *Hamp* mRNA levels and Fpn1 expression in RES macrophages and duodenal epithelial cells. Aged cohorts of *Pcm* mutant mice exhibited an iron-deficient erythropoiesis in the context of profound iron sequestration in RES macrophages and other cell types, constituting the end point of *Pcm* disease pathogenesis.

EXPERIMENTAL PROCEDURES

Mice and Genotyping—*Pcm* mice on a partially congenic A/J background (N5 and later) were used for analysis and genotyped as described previously (3). Cohorts of *Pcm* and wild-type animals were aged to 8–19 months and fed a standard chow. All animal experiments in this study were approved by the Institutional Animal Care and Use Committee of Baylor College of Medicine.

Microarray Analysis—Total RNA was isolated from liver and duodenum samples using TRIzol reagent (Invitrogen) and prepared according to standard methods. Pools of total liver RNA from 6 *Pcm* heterozygotes and 6 wild-type mice at 3, 7, and 12 weeks of age were analyzed using the Mouse Version 6.0 of the IronChip as described previously (11). Likewise, pools of total duodenal RNA from 6 *Pcm* heterozygotes and 6 wild-type mice were analyzed at 7 and 12 weeks of age. Expression values were calculated from dye swap experiments (18). Genes were represented by either single or multiple clones on the microarray platform. In the latter case, the average ratios and standard deviations were determined. The entire data set representing the expression values of all genes represented on the IronChip cDNA microarray platform will be submitted to Array express (European Bioinformatics Institute).

Real-time RT-PCR Analysis—Reactions and signal detection were performed on an ABI Prism 7000 sequence detection system (Applied Biosystems) using the following primers: *Fpn1* (Mm00489837_m1), *Hamp* (Mm00519025_m1), *Trfr* (Mm00441941_m1), *Slc11a2* (Mm00435363_m1), and *Rgmc* (Mm00510148_s1) (all from Applied Biosystems). 18 S rRNA assay was conducted using primers 5′-TCGAGGCCCTGTAATTGGAA-3′ (forward), 5′-CCCTCCAATGGATCCTCGTT-3′ (reverse), and TaqMan MGB probe 5′-AGTCCACTTTAAATCCTT-3′ labeled with VIC (Applied Biosystems). mRNA levels were expressed as a difference of cycles to threshold (ΔCT) between the gene-specific probe and 18 S standard; mean wild-type values were centered at zero.

Histology and Immunohistochemistry—Liver and duodenal samples from various stages were processed as described previously (3). A polyclonal Fpn1 antibody was generated in rabbit against oligopeptide sequence GPDEKEVTDENQPNTS at the carboxyl terminus of Fpn1 and immunoaffinity purified. Immunohistochemistry for Fpn1 and F4/80 (clone CI:A3–1; Serotec) was performed as described (4). For Trfr antigen retrieval, sections were boiled in 0.01 M citric acid, pH 6.0, and blocking was achieved with horse serum. Primary antibody incubation was performed overnight at 4 °C using mouse α-TfR at 1:1000 dilution (Invitrogen). Prussian blue staining for iron was accomplished using the Accustain iron staining kit (Sigma) according to the manufacturer's protocol. For comparison of protein expression levels, wild-type and *Pcm* mutant samples were mounted side by side on the same slide. Images were acquired with a Sony 085 CCD color RGB sensor digital camera mounted on a Zeiss Axioplan 2 microscope.

Iron Determination and Blood Cell Analyses—Non-heme tissue and serum iron were determined as described previously (3). Hematocrit (Hct) measurements, expressed as a percentage, were obtained by standard microcapillary determination. Red cell parameters, including mean corpuscular volume and mean corpuscular hemoglobin concentration, as well as white blood cell (WBC) counts were determined on the ADVIA 120 hematology system (Bayer).

Statistical Analyses—All data are reported as the mean ± S.D. All comparisons were made *versus* wild-type cohorts and analyzed for significant differences using the Student's unpaired *t*-test.

RESULTS

To elucidate the consequences of dynamic *Fpn1* dysregulation on the genetic circuitry governing iron metabolism, oxidative stress, hypoxia, and inflammation we used a highly sensitive and accurate cDNA microarray platform, the IronChip (11). The analysis focused on gene expression in liver and duodenum, respectively, as sites of iron storage and absorption at 3, 7, and 12 weeks of age. In the context of the striking polycythaemia phenotype by young adulthood, heretofore not described in animal models of dysregulated iron metabolism, molecular analyses were directed toward *Pcm* heterozygotes. In comparison with previous microarray studies on mouse models of iron balance abnormalities (11, 19), *Pcm* mice presented discrete but highly reproducible differences in hepatic and duodenal gene expression during postnatal development (Fig. 1). To validate the microarray findings based on pooled RNA, the individual samples were subjected to real-time RT-PCR analysis using the most relevant probes. The average changes of differential gene expression along with the respective standard deviations are shown in supplemental Table S1.

The Hamp-Fpn1 Homeostatic Loop—Neither microarray analysis nor quantitative RT-PCR detected statistically significant differences in duodenal and hepatic *Fpn1* transcript levels between *Pcm* heterozygous and wild-type mice at 3, 7, and 12 weeks of age (Figs. 1 and 2, *A* and *B*). The lack of *Fpn1* transcript up-regulation in 7-week *Pcm* heterozygous liver demonstrated a post-transcriptional mechanism of Fpn1 protein up-regulation in polycythaemic *Pcm* heterozygotes (3).

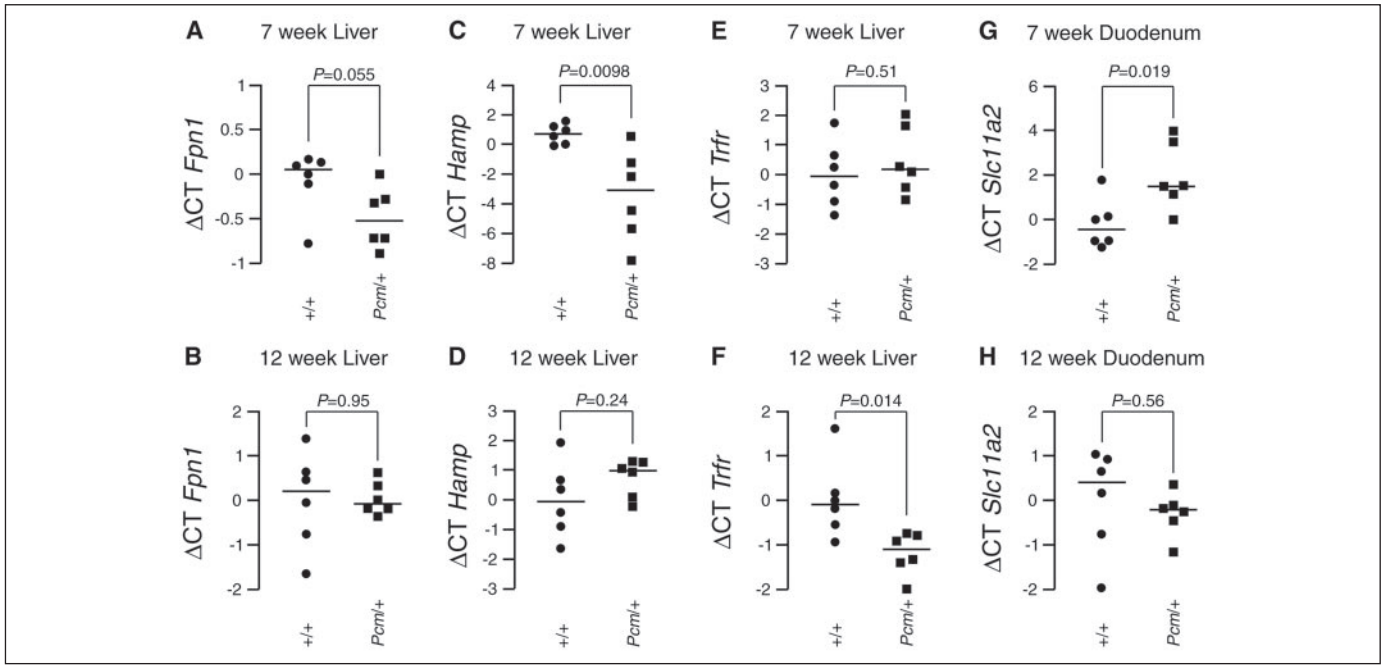

FIGURE 2. **Quantitative real-time RT-PCR analyses for *Fpn1*, *Hamp*, *Trfr*, and *Slc11a2*.** No statistically significant differences for liver *Fpn1* mRNA levels were observed at 7 (*A*) or 12 (*B*) weeks. *Hamp* expression in liver was lower in *Pcm* heterozygotes at 7 weeks (*C*) but not at 12 weeks (*D*). Conversely, no difference in *Trfr* mRNA levels in liver was detected at 7 weeks (*E*), but mRNA levels were statistically significantly lower in *Pcm* heterozygotes at 12 weeks (*F*). *Pcm* heterozygotes presented higher *Slc11a2* expression in the duodenum at 7 (*G*) but not at 12 (*H*) weeks. *Horizontal lines* depict median values.

Importantly, hepatic *Hamp* mRNA levels were significantly reduced in *Pcm* heterozygotes at 7 weeks of age (Figs. 1 and 2*C*). However, this reflected a delay in developmental *Hamp* up-regulation because at 12 weeks of age *Hamp* mRNA levels in *Pcm* heterozygotes were significantly higher (microarrays) or similar (RT-PCR) to wild-type levels (Figs. 1 and 2*D*). Thus, delayed developmental up-regulation of Hamp is conducive to persistent elevation in Fpn1 protein expression in polycythaemic 7-week *Pcm* heterozygotes (3). These results underscore the responsiveness of *Hamp* regulation to the dynamic changes in hepatic iron levels in the context of the *Fpn1* regulatory allele. Therefore, to the best of our knowledge, the *Pcm* mouse model provides the strongest evidence to date for the Hamp-Fpn1 homeostatic loop *in vivo*.

Interestingly, despite statistically significant down-regulation of hepatic *Hamp* levels in polycythaemic 7-week-old *Pcm* heterozygotes, no difference in mRNA expression of *Rgmc,* the mouse homolog of Hemojuvelin and potential upstream regulator of Hamp (20), was observed in liver (*Pcm*/+ ΔCT *Rgmc* 0.39 ± 0.46 ($n = 6$) *versus* +/+ ΔCT *Rgmc* 0 ± 0.83 ($n = 6$); $p = 0.33$). These results support recent evidence for differential regulation of *Hamp* and *Rgmc* in response to iron balance or erythropoietin application (21).

Response Patterns of Iron Metabolism Genes—In good agreement with the severe neonatal iron deficiency in *Pcm* mice (3, 4), microarray analysis detected increased hepatic *Trfr* (transferrin receptor) mRNA expression in 3- and 7-week-old *Pcm* heterozygotes (Fig. 1). Quantitative RT-PCR showed no statistically significant difference between *Pcm* heterozygotes and wild-type controls at 7 weeks (Fig. 2*E*). However, both the IronChip and quantitative RT-PCR demonstrated a strong decrease in *Trfr* mRNA expression by 12 weeks of age (Figs. 1 and 2*F*). This result is consistent with destabilization of *Trfr* mRNA by a mechanism dependent on iron regulatory proteins (1) in response to hepatic iron accumulation in *Pcm* liver at 12 weeks of age (3), obviating Trfr-dependent cellular iron uptake. Likewise, increased *Hmox1* (*heme oxygenase 1*) mRNA levels in 7- and 12 week-old *Pcm* heterozygotes can be explained by the increased need for heme catabolism in polycythaemic animals, heralding hepatic iron accumulation (Fig. 1). Consistent with marked systemic iron requirement and low hepatic *Hamp* mRNA expression, duodenal *Trfr*, *cybrd1* (duodenal cytochrome *b*), and *Slc11a2* (solute carrier 11a2; also known as *Nramp2*, *Dmt1*) mRNA levels of *Pcm* heterozygotes at 7 weeks of age were increased (Figs. 1 and 2*G*). Increased expression of these iron transporters reverted to wild-type levels at 12 weeks of age (Figs. 1 and 2*H*). Therefore, coordinated shifts in transcriptional expression patterns of these genes are sufficient to explain the transitory iron loading in *Pcm* heterozygotes.

Response Patterns of Selected Iron Metabolism Proteins in Liver and Duodenum—At 3 weeks of age, Trfr was expressed at moderate levels in wild-type liver, whereas *Pcm* heterozygotes displayed significant up-regulation of this protein (Fig. 3*A;* compare with mRNA results in Fig. 1). Inspection under high magnification suggested significant augmentation of Trfr levels in Kupffer cells and sinusoidal endothelial cells, contrasting with a more subtle increase in expression in hepatocytes (data not shown). At 12 weeks, *Pcm* heterozygotes demonstrated significantly lower Trfr levels compared with wild-type liver (Fig. 3*B*), consistent with the mRNA results (Fig. 1). Elevated Trfr protein expression in duodenum from 7-week-old *Pcm* heterozygotes restored Trfr to levels indistinguishable from wild-type littermates at 12 weeks of age (Fig. 3, *C* and *D*; compare with mRNA results in Fig. 1). Thus, immunohistochemistry corroborated the *Trfr* mRNA response patterns in liver and duodenum. At 7 weeks of age, *Pcm* heterozygous duodenum exhibited significant elevation of Fpn1 expression compared with wild-type littermates (Fig. 3*E*). Increased expression was particularly evident at the basolateral membrane of the epithelial cells. Conversely, at 12 weeks of age, *Pcm* heterozygotes were remarkable for markedly lower Fpn1 expression levels compared with wild-type (Fig. 3*F*). Because *Fpn1* mRNA levels were indistinguishable between *Pcm* heterozygotes and wild-type at both 7 and 12 weeks of age (Fig. 1), the changes in protein levels strongly supported the notion of Hamp-mediated post-translational regulation of Fpn1 expression.

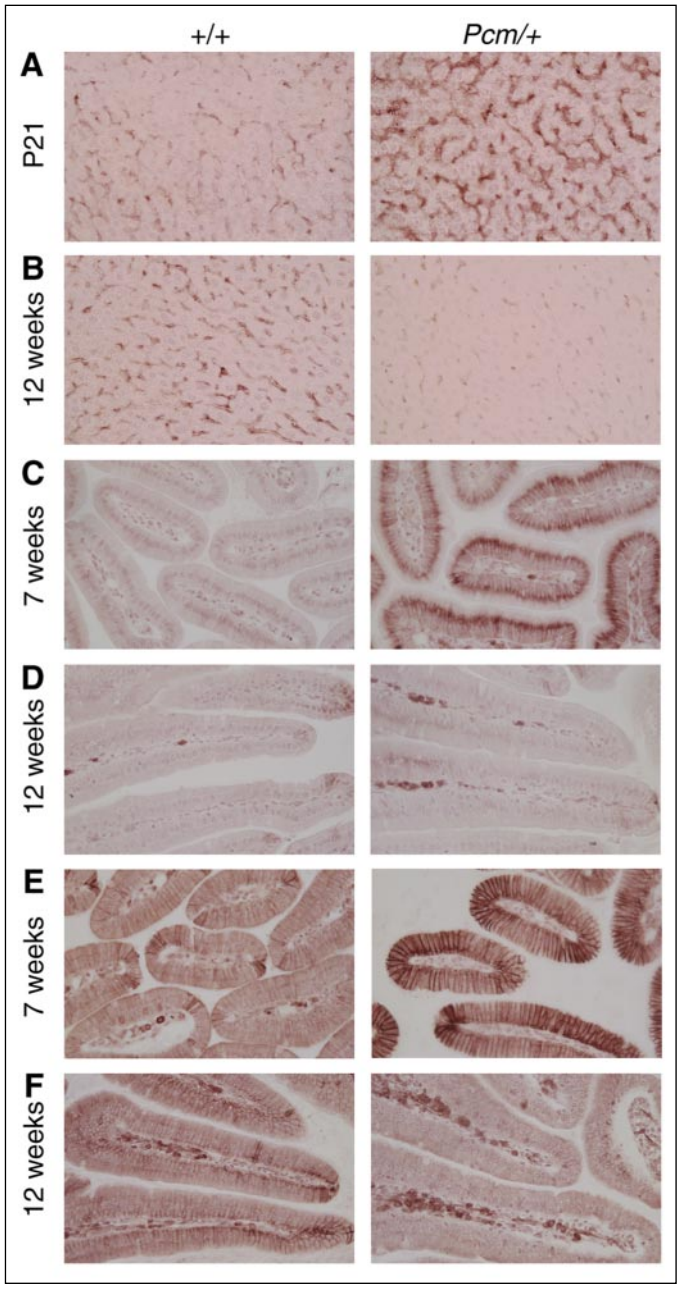

FIGURE 3. **Trfr and Fpn1 expression in *Pcm* liver and duodenum.** Immunohistochemistry detected higher levels of Trfr expression in *Pcm* heterozygous liver at 3 weeks of age compared with wild-type (*A*). Conversely, expression of Trfr in *Pcm* heterozygotes was significantly lower at 12 weeks compared with wild-type liver (*B*). Augmented Trfr expression in 7-week *Pcm* heterozygous duodenum (*C*) reverted to wild-type levels by 12 weeks of age (*D*). Immunohistochemistry for Fpn1 revealed elevated expression in 7-week duodenum from *Pcm* heterozygotes compared with wild-type (*E*). Note the distinct Fpn1 expression along the basolateral membrane of the epithelial cells. In contrast, at 12 weeks of age, *Pcm* heterozygotes demonstrated lower levels of Fpn1 expression compared with wild-type duodenum (*F*). Original magnification ×400 for all panels.

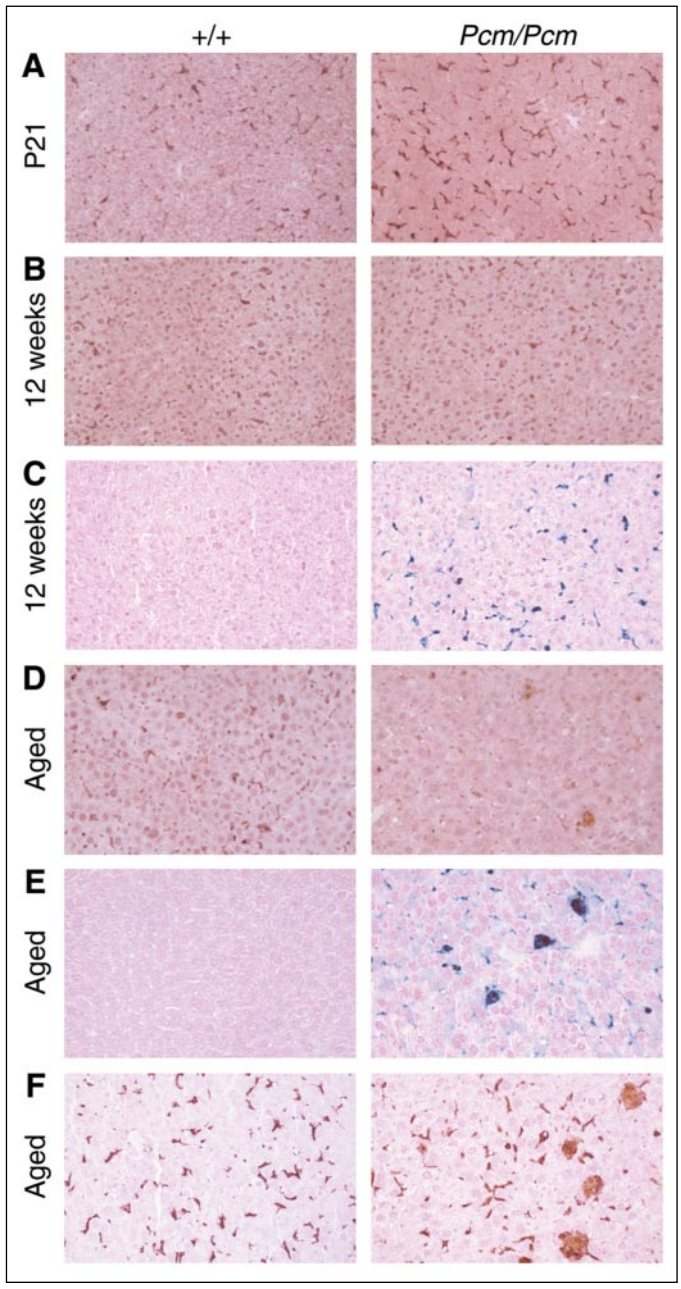

FIGURE 4. **Fpn1 expression and iron overload in *Pcm* liver.** Compared with wild-type, immunohistochemistry detected increased levels of Fpn1 expression in Kupffer cells in 3-week-old *Pcm* homozygotes (*A*), whereas no differences were observed b y 12 weeks of age (*B*). Prussian blue staining revealed iron accumulation in Kupffer cells in 12-week liver of *Pcm* homozygotes (*C*). By immunohistochemistry, Fpn1 expression remained near base-line levels in aged *Pcm* homozygous liver (*D*), whereas Prussian blue staining showed significant iron accumulation, predominantly in Kupffer cells (*E*). Immunohistochemistry for F4/80 revealed a similar distribution and number of macrophages in livers from aged wild-type and *Pcm* homozygous animals (*F*). Original magnification ×200 for all panels.

Down-regulation of Fpn1 Expression and Reticuloendothelial Iron Overload—We previously demonstrated a significant augmentation of Fpn1 protein expression in *Pcm* mutant liver during early postnatal development (3). By immunohistochemistry, increased Fpn1 expression localized predominantly to punctate, stellate-shaped cells at 3 weeks of age (Fig. 4*A*). Based on a similar staining pattern for F4/80 (data not shown), the antibody to which recognizes a macrophage-restricted glycoprotein of the epidermal growth factor 7 family (22), marked up-regulation of Fpn1 in *Pcm* mutants localized to Kupffer cells. Likewise, persistent elevation of Fpn1 protein expression at 7 weeks of age localized predominantly to Kupffer cells in polycythaemic *Pcm* heterozygotes (data not shown). In contrast, the small subset of *Pcm* heterozygotes with normal hematocrit as well as *Pcm* homozygotes displayed wild-type levels of hepatic Fpn1 expression (data not shown). By 12 weeks of age, the Fpn1 expression pattern was indistinguishable between wild-type and *Pcm* mutant liver (Fig. 4*B*). This down-regulation of Fpn1 expression correlated with RES iron accumulation in *Pcm* homozygous liver by 12 weeks of age (Fig. 4*C*). Furthermore, hepatic

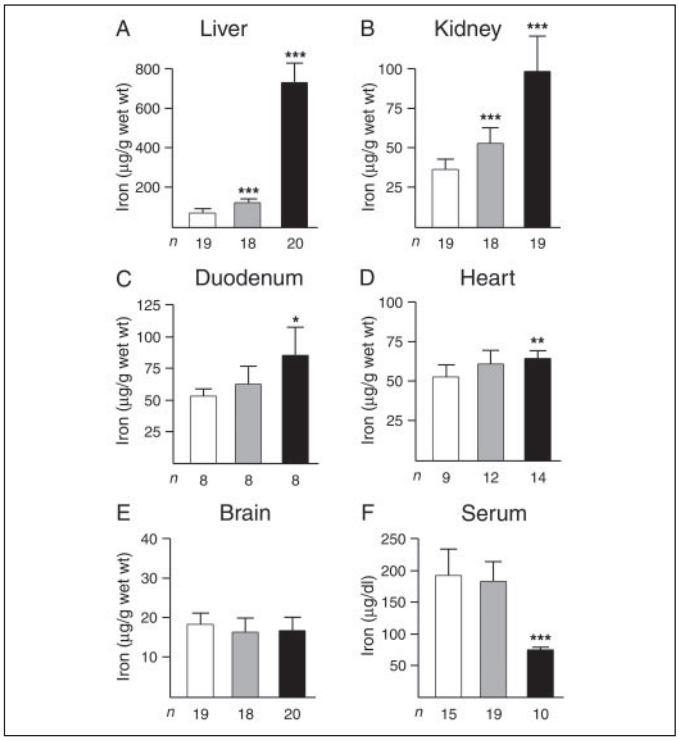

FIGURE 5. **Iron levels in aged *Pcm* mice.** Non-heme iron levels were elevated in *Pcm* mutant liver (*A*), kidney (*B*), duodenum (*C*), and heart (*D*). Although no differences in non-heme iron levels were observed in brain (*E*), *Pcm* homozygotes showed decreased serum iron levels (*F*). *White columns* depict wild-type; *gray columns Pcm* heterozygous; *black columns Pcm* homozygotes. *, $p < 0.01$; **, $p < 0.001$; ***, $p < 0.0001$.

Fpn1 expression remained near base-line levels in aged *Pcm* homozygotes (Fig. 4*D*), whereas significant iron accumulation persisted (Fig. 4*E*). Large accumulations of iron, consistent with hemosiderosis, were observed in cells staining against F4/80 (Fig. 4*F*). Notably, the overall number of macrophages appeared similar between aged wild-type and mutant livers (Fig. 4*F*), and collagen staining revealed no evidence of widespread fibrosis (data not shown).

The Disease End Point in Aged Pcm Animals—Several parameters of iron homeostasis were determined in *Pcm* mice between 8 and 19 months of age. Analysis of age subgroups did not reveal any phenotypic difference, indicating that by 8 months of age all *Pcm* mice had reached the disease end point (data not shown). Hepatic iron levels remained many-fold elevated in aged *Pcm* animals (Fig. 5*A*) in a predominantly punctate pattern of distribution (Fig. 4*E*). Other tissues, including kidney (Fig. 5*B*), duodenum (Fig. 5*C*), and heart (Fig. 5*D*), also demonstrated significant elevation in iron content. Strikingly, no difference in brain iron levels was observed in aged *Pcm* mutants (Fig. 5*E*). This was also observed in the context of normal brain iron balance in humans with hereditary hemochromatosis or secondary iron overload (23). Importantly, serum iron levels were significantly reduced in aged *Pcm* homozygotes (Fig. 5*F*). Microcapillary determination of Hct revealed a graded severity of anemia in aged *Pcm* mutants (+/+ Hct 39.9 ± 1.8% ($n = 19$); *Pcm*/+ Hct 35.0 ± 3.4% ($n = 16$), $p < 0.0001$; *Pcm/Pcm* Hct 32.5 ± 2.2% ($n = 22$); $p < 0.0001$). *Pcm* homozygotes also displayed significant microcytosis (*Pcm*/*Pcm* mean corpuscular volume 41.5 ± 1.3 fl ($n = 17$) *versus* +/+ mean corpuscular volume 52.1 ± 4.0 fl ($n = 15$); $p < 0.0001$); no differences in mean corpuscular hemoglobin concentration were observed (data not shown). Consistent with RES iron accumulation and reduced serum iron levels in aged animals, real-time RT-PCR analysis of hepatic *Hamp* transcript levels revealed a trend toward increased expression, albeit not at statistically significant levels (+/+ ΔCT *Hamp* 0 ± 3.27 ($n = 8$); *Pcm*/+ ΔCT *Hamp* 1.74 ± 0.61 ($n = 7$), $p = 0.19$; *Pcm/Pcm* ΔCT *Hamp* 1.84 ± 0.74 ($n = 8$); $p = 0.14$).

Red cell parameters and white blood cell counts in aged cohorts of *Pcm* animals are shown in supplemental Table S2. A modest but significant elevation in WBC was observed in both heterozygotes (*Pcm*/+ WBC 1.2 ± 0.42 10^3 cells/µl ($n = 10$) *versus* +/+ WBC 0.87 ± 0.32 10^3 cells/µl ($n = 15$); $p = 0.027$) and homozygotes (*Pcm/Pcm* WBC 1.7 ± 0.99 10^3 cells/µl ($n = 17$); $p = 0.0044$). This was primarily reflective of an increase in absolute lymphocyte count and, to a lesser degree, neutrophil count. No statistically significant differences in monocyte, eosinophil, or basophil counts were observed. In the context of a semidominant defect in spleen development in *Pcm* animals (4), it is conceivable that the increased presence of circulating white blood cells in aged *Pcm* mice results from the defects in this significant repository site for immune cells.

DISCUSSION

In recent years, positional cloning of iron disease loci in both humans and mutant mouse models, complemented by transgenic and gene knock-out studies in mice, have identified many genes involved in iron metabolism (1). The challenge now resides in dissecting the function of the encoded proteins and their integration into the regulatory circuits governing cellular and organismal iron homeostasis. These investigations will benefit greatly from the availability of mouse strains, such as *Pcm*, with regulatory mutations in critical components of the pathways.

The *Pcm* mouse mutant exhibits the gamut of iron balance disorders, ranging from iron deficiency at birth to tissue iron overload by young adulthood (3, 4). The present study defined, in molecular terms, the regulatory interferences underlying the dynamic changes in iron homeostasis in *Pcm* mice. For example, duodenal and/or hepatic expression of Fpn1 and Trfr protein, as well as *Hamp*, *cybrd1* and *Slc11a2* mRNA, explained the transition from early postnatal iron deficiency to iron overload in 12-week old *Pcm* mice. In comparison with previous studies (10, 11), these results demonstrate transcriptional responsiveness of the duodenal iron transport system to organismal and/or cellular iron balance. These changes in gene expression are likely to result directly or indirectly from alterations in Hamp signaling. Recently, it was shown that, under conditions of augmented erythropoiesis and decreased Hamp expression, mRNA and protein levels of Slc11a2 and Cybrd1 increased (24). Furthermore, genetically *Hamp*-deficient mice demonstrated up-regulation of Slc11a2, Cybrd1, and Fpn1 expression (25). Our results indicate that polycythaemic 7-week-old *Pcm* heterozygotes demonstrate decreased *Hamp* expression in the context of significant alterations in mRNA levels of iron-related genes, such as iron transporters. In addition, cellular regulation responsive to Fpn1-mediated elevated iron efflux from intestinal enterocytes leading to increased mRNA expression of iron transporters in *Pcm* heterozygotes must be considered (26).

Genetic evidence suggests that *Rgmc,* a second causative gene for juvenile onset hereditary hemochromatosis (type II), functions upstream of Hamp (20). Conceivably, profound down-regulation of *Hamp* in polycythaemic *Pcm* heterozygotes at 7 weeks of age constitutes an appropriate *in vivo* context to discern expression differences in putative upstream regulators, including *Rgmc*. However, mRNA levels of *Rgmc* were indistinguishable between wild-type and 7-week old *Pcm* heterozygotes. Similarly, work by Krijt *et al.* (21) revealed no differences in *Rgmc* transcript levels following treatment of mice with iron or erythropoietin, known regulators of *Hamp* expression. Thus, *Hamp* regulation in response to iron status is not likely to depend on changes in *Rgmc* transcription.

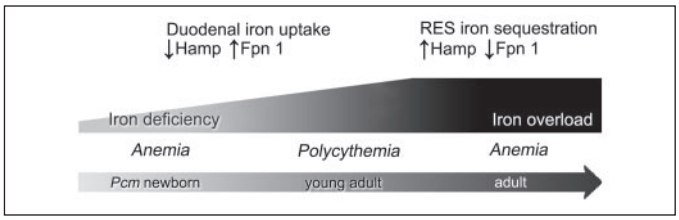

FIGURE 6. **Model for dynamic changes in iron homeostasis in *Pcm* mice.** *Horizontal bar* represents the organismal iron balance. Alterations in the Hamp-Fpn1 homeostatic loop and iron balance are represented relative to hematopoietic phenotypes and developmental stages.

Recently, it was shown that *Hamp* expression is regulated developmentally (21). Compared with fetal development, perinatal *Hamp* expression decreases by the order of several magnitudes, reaching lowest levels by P8. As postnatal development proceeds, *Hamp* levels gradually return to high levels by adulthood. Fig. 6 depicts a model wherein delayed up-regulation of *Hamp* in the context of increased *Fpn1* mRNA translation from iron-responsive element-less transcripts (3) forms the basis for elevated Fpn1 protein levels, governing *Pcm* pathogenesis during early postnatal development. Therein, dysregulated Fpn1-mediated duodenal uptake overcompensates for the perinatal iron deficiency and causes organismal iron overload. Upon up-regulation of *Hamp* by 12 weeks of age, Fpn1 levels decrease in a distinctly post-transcriptional manner, iron uptake ceases, and iron becomes increasingly sequestered in RES macrophages and duodenal epithelial cells. This heralds the *Pcm* disease end point at a fairly early stage, because aged cohorts of *Pcm* mutant mice exhibited an iron-deficient erythropoiesis in the context of marked iron sequestration in RES macrophages, duodenum, and other tissues, as well as reduced serum iron levels. Similar to the anemia of chronic disease caused by other disease mechanisms (27), it remains an enigma why signaling through the iron-deficient erythron is insufficient to reverse Hamp up-regulation and thus ameliorate iron sequestration and anemia in aged *Pcm* mice. Nonetheless, iron-deficient erythropoiesis marks both the beginning and the end point of the hematopoietic defects in *Pcm* mice. However, whereas embryonic/perinatal anemia results from primary organismal iron deficiency (4), adult *Pcm* mice develop anemia because of decreased iron bioavailability despite organismal iron overload. The polycythaemia develops at the transition phase between the two disease states, governed by unimpeded erythropoietin signaling (3).

Recent studies have described several mechanisms by which mutations in human FPN could lead to type IV hereditary hemochromatosis, including unresponsiveness to Hamp-mediated degradation, defects in cell surface localization, and dominant-negative effects on cellular processing of wild-type FPN (28–31). Phenotypic and molecular analyses of *Pcm* mice support an additional disease mechanism wherein augmented Fpn1-mediated iron uptake earlier in life is followed by RES iron sequestration and microcytic anemia due to homeostatic Hamp signaling. Interestingly, a loss-of-function mutation in Fpn1 did not result in significant hepatic iron overload in heterozygous mice (5). Therefore, to the best of our knowledge, *Pcm* represents the first *in vivo* model system demonstrating disease end points commonly detected in type IV hemochromatosis. Additionally, the present results suggest that, due to the dynamic nature of iron homeostasis, analyses of *in vivo* models should require consideration of various stages in pre- and postnatal development as the phenotypic richness and regulatory intricacies cannot be appreciated by the description of one or two stages alone.

Acknowledgments—We thank Dr. Josef Prchal and members of our laboratories for helpful discussions and critical reading of the manuscript.

REFERENCES

1. Hentze, M. W., Muckenthaler, M. U. & Andrews, N. C. (2004) *Cell* **117,** 285–297
2. Knutson, M. & Wessling-Resnick, M. (2003) *Crit. Rev. Biochem. Mol. Biol.* **38,** 61–88
3. Mok, H., Jelinek, J., Pai, S., Cattanach, B. M., Prchal, J. T., Youssoufian, H. & Schumacher, A. (2004) *Development* **131,** 1859–1868
4. Mok, H., Mendoza, M., Prchal, J. T., Balogh, P. & Schumacher, A. (2004) *Development* **131,** 4871–4881
5. Donovan, A., Lima, C. A., Pinkus, J. L., Pinkus, G. S., Zon, L. I., Robine, S. & Andrews, N. C. (2005) *Cell Metabol.* **1,** 191–200
6. Abboud, S. & Haile, D. J. (2000) *J. Biol. Chem.* **275,** 19906–19912
7. McKie, A. T., Marciani, P., Rolfs, A., Brennan, K., Wehr, K., Barrow, D., Miret, S., Bomford, A., Peters, T. J., Farzaneh, F., Hediger, M. A., Hentze, M. W. & Simpson, R. J. (2000) *Mol. Cell* **5,** 299–309
8. Zoller, H., Theurl, I., Koch, R., Kaser, A. & Weiss, G. (2002) *Blood Cells Mol. Dis.* **29,** 488–497
9. Martini, L. A., Tchack, L. & Wood, R. J. (2002) *J. Nutr.* **132,** 693–696
10. Dupic, F., Fruchon, S., Bensaid, M., Loreal, O., Brissot, P., Borot, N., Roth, M. P. & Coppin, H. (2002) *Gut* **51,** 648–653
11. Muckenthaler, M., Roy, C. N., Custodio, A. O., Minana, B., deGraaf, J., Montross, L. K., Andrews, N. C. & Hentze, M. W. (2003) *Nat. Genet.* **34,** 102–107
12. Adams, P. C., Barbin, Y. P., Khan, Z. A. & Chakrabarti, S. (2003) *Blood Cells Mol. Dis.* **31,** 256–261
13. Bridle, K. R., Frazer, D. M., Wilkins, S. J., Dixon, J. L., Purdie, D. M., Crawford, D. H., Subramaniam, V. N., Powell, L. W., Anderson, G. J. & Ramm, G. A. (2003) *Lancet* **361,** 669–673
14. Knutson, M. D., Vafa, M. R., Haile, D. J. & Wessling-Resnick, M. (2003) *Blood* **102,** 4191–4197
15. Liu, X. B., Hill, P. & Haile, D. J. (2002) *Blood Cells Mol. Dis.* **29,** 315–326
16. Nemeth, E., Tuttle, M. S., Powelson, J., Vaughn, M. B., Donovan, A., Ward, D. M., Ganz, T. & Kaplan, J. (2004) *Science* **306,** 2090–2093
17. Pietrangelo, A. (2004) *Blood Cells Mol. Dis.* **32,** 131–138
18. Richter, A., Schwager, C., Hentze, S., Ansorge, W., Hentze, M. W. & Muckenthaler, M. (2002) *BioTechniques* ***33,*** 620–628, 630
19. Muckenthaler, M., Richter, A., Gunkel, N., Riedel, D., Polycarpou-Schwarz, M., Hentze, S., Falkenhahn, M., Stremmel, W., Ansorge, W. & Hentze, M. W. (2003) *Blood* **101,** 3690–3698
20. Celec, P. (2005) *J. Mol. Med.* **83,** 521–525
21. Krijt, J., Vokurka, M., Chang, K. T. & Necas, E. (2004) *Blood* **104,** 4308–4310
22. McKnight, A. J., Macfarlane, A. J., Dri, P., Turley, L., Willis, A. C. & Gordon, S. (1996) *J. Biol. Chem.* **271,** 486–489
23. Ponka, P. (2004) *Ann. N. Y. Acad. Sci.* **1012,** 267–281
24. Latunde-Dada, G. O., Vulpe, C. D., Anderson, G. J., Simpson, R. J. & McKie, A. T. (2004) *Biochim. Biophys. Acta* **1690,** 169–176
25. Viatte, L., Lesbordes-Brion, J. C., Lou, D. Q., Bennoun, M., Nicolas, G., Kahn, A., Canonne-Hergaux, F. & Vaulont, S. (2005) *Blood* **105,** 4861–4864
26. Frazer, D. M. & Anderson, G. J. (2003) *Blood Cells Mol. Dis.* **30,** 288–297
27. Jurado, R. L. (1997) *Clin. Infect. Dis.* **25,** 888–895
28. Drakesmith, H., Schimanski, L. M., Ormerod, E., Merryweather-Clarke, A. T., Viprakasit, V., Edwards, J. P., Sweetland, E., Bastin, J. M., Cowley, D., Chinthammitr, Y., Robson, K. J. & Townsend, A. R. (2005) *Blood* **106,** 1092–1097
29. Schimanski, L. M., Drakesmith, H., Merryweather-Clarke, A. T., Viprakasit, V., Edwards, J. P., Sweetland, E., Bastin, J. M., Cowley, D., Chinthammitr, Y., Robson, K. J. & Townsend, A. R. (2005) *Blood* **105,** 4096–4102
30. Liu, X. B., Yang, F. & Haile, D. J. (2005) *Blood Cells Mol. Dis.* **35,** 33–46
31. De Domenico, I., Ward, D. M., Nemeth, E., Vaughn, M. B., Musci, G., Ganz, T. & Kaplan, J. (2005) *Proc. Natl. Acad. Sci. U. S. A.* **102,** 8955–8960